

Effective thermalization of a many-body dynamically localized Bose gas

Vincent Vuatelet¹ and Adam Rançon¹

¹*Université de Lille, CNRS, UMR 8523 – PhLAM – Laboratoire de Physique des Lasers, Atomes et Molécules, F-59000 Lille, France*

(Dated: October 6, 2021)

Dynamical localization is the analog of Anderson localization in momentum space, where the system’s energy saturates and the single-particle wave-functions are exponentially localized in momentum space. In the presence of interactions, in the context of a periodically kicked Bose gas, it has been argued that dynamical localization persists. Focusing on the Tonks (strongly interacting) regime, we show that the many-body dynamically localized phase is effectively thermal, a clear deviation from the breaking of ergodicity observed in standard many-body localized systems. We relate the effective temperature to the driving parameters, and thus quantitatively describe the loss of coherence at large distances in this phase. Contrary to the non-interacting case, the momentum distribution decays as a power-law at large momenta, characterized by an effectively thermal Tan’s contact. This is a rare example where driving and many-body (dynamical) localization lead to an effectively ergodic state.

I. INTRODUCTION

Anderson localization of classical and quantum waves is a universal phenomenon induced by disorder [1, 2]. Whether or not it survives in the presence of interactions has been under intense scrutiny in recent years, both theoretically and experimentally [3, 4]. It is now well understood that while interactions tend to destroy localization, a strong enough disorder will give rise to Many-Body Localization (MBL), at least in low dimensions. MBL can be understood in terms of an effective integrability due to the existence of an extensive number of local integrals of motions, breaking ergodicity and preventing thermalization [5, 6]. The same mechanism prevents driven MBL systems from absorbing an infinite amount of energy and thus prevents runaway heating [7, 8].

Dynamical localization is the quantum chaos analog of Anderson localization, but taking place in momentum space [9]. In the paradigmatic quantum kicked rotor (QKR), periodic kicks give rise to a ballistic propagation in momentum space, while the (pseudo) random phase accumulated during the free propagation in between kicks by each momentum state plays the role of disorder, resulting in destructive quantum interferences and dynamical localization. Experimental realizations of the atomic QKR have allowed for detailed investigations of the Anderson physics: observation of Anderson transition [10], characterization of its critical properties [11, 12], localization at the upper critical dimension [13], the effects symmetries on weak localization [14], and classical-to-quantum transition at early times [15].

Whether interactions destroy dynamical localization is a fundamental question that challenges our understanding of driven interacting quantum systems. This has been studied for various toy-models [16–21], as well as for the kicked Lieb-Liniger model, a realistic model for cold atoms experiments [22]. At the mean-field level, it has been argued both on theoretical and numerical grounds that interactions destroy dynamical localization, which is replaced by a subdiffusion in momentum space [23–28].

However, it is well known that mean-field theory breaks down in one dimension [29], questioning these predictions. Beyond mean-field, an early study for two bosons hinted that interactions may also destroy dynamical localization [30], but the validity of these results has been recently questioned [31]. Finally, Rylands et al. have argued that dynamical localization persists in the presence of interactions, leading to a Many-Body Dynamically Localized (MBDL) phase [32]. The MBDL phase can be described by a steady-state density matrix $\hat{\rho}_{ss}$, which in general should belong to a generalized Gibbs ensemble [33, 34]. However, this regime and its density matrix have yet to be characterized.

In this article, we study the MBDL phase of the kicked Lieb-Liniger gas in the infinite interaction (Tonks) regime. Our main result is that the steady-state of the system is very well described by the density matrix of a *thermal* gas, seemingly in contradiction with the fact that the system is integrable and has an extensive number of conserved charges (the occupation of the Floquet eigenstates). We stress that this effective thermalization takes place while the system is still periodically driven. This is a rare instance where driving and Many-Body (Dynamical) Localization give rise to an effectively ergodic state. We relate this temperature to the system’s parameters (kicks strength and period). This allows us to quantitatively characterize two experimentally relevant observables: the momentum distribution that does not decay exponentially, as in the non-interacting limit, but as a power-law, which is to be expected for interacting quantum systems [35, 36]; and the coherence function, which decays exponentially, demonstrating the absence of phase coherence.

The article is organized as follows. Sec. II, we present the model and the physical observables studied. In Sec. III, we summarize our numerical results for the momentum distribution and the coherence function in the localized regime, while in Sec. IV we interpret those results in terms of an effective thermalization of the system, and we give arguments to explain such a thermalization

in Sec. V. The discussion of our results appears in Sec. VI.

II. MODEL

We consider N interacting bosons of mass m , the dynamics of which is described by the periodic Hamiltonian

$$\hat{H}(t) = \sum_i \left(\frac{\hat{p}_i^2}{2} + K \cos(\hat{x}_i) \sum_n \delta(t-n) \right) + g \sum_{i<j} \delta(\hat{x}_i - \hat{x}_j). \quad (1)$$

The one-body term corresponds to the QKR Hamiltonian $\hat{H}_{QKR}(t)$, while the other describes the contact interaction (we also define $\hat{H}_{TG} = \hat{H}|_{K=0}$). Here and in the following, time is in units of the period τ of the kicks and length in unit of the inverse of the kick-potential wavenumber k_K . Momenta are normalized such that $[\hat{x}_i, \hat{p}_j] = ik\delta_{ij}$, with $k = \hbar k_K^2 \tau / m$ the effective Planck constant. The system is of size $L = 2\pi$, and we assume periodic boundary conditions, implying that momenta are quantized in unit of k (we will use units such that the Boltzmann constant $k_B = 1$).

In the free case ($g = 0$), we recover the physics of the QKR, where any single-particle wave-function is localized in momentum space at long time (larger than the localization time) and decays exponentially in momentum space, with the same ‘‘localization length’’ p_{loc} (for larger K/k , one finds $p_{loc} \propto K^2/k$ [37, 38]) [39]. In particular, the total energy of the system saturates to a constant value at long time.

Here, we focus on the Tonks regime, $g \rightarrow \infty$, allowing us to write the exact time-dependent wave-function $\Psi_B(\{x\}; t)$ of the system using the Bose-Fermi mapping [40–44],

$$\Psi_B(\{x\}; t) = \prod_{i<j} \text{sign}(x_i - x_j) \Psi_F(\{x\}; t), \quad (2)$$

where $\Psi_F(\{x\}; t) = \frac{1}{\sqrt{N!}} \det[\psi_i(x_j, t)]$ is the free fermions wave-function constructed from the N single-particle orbitals $\psi_i(x, t)$, which evolve according to the QKR Hamiltonian, $ik\partial_t |\psi_i(t)\rangle = \hat{H}_{QKR}(t) |\psi_i(t)\rangle$. We assume that the system starts in its ground state, i.e. the fermionic wave-function describes a Fermi sea with Fermi momentum $p_F \propto N$ and ground state energy E_0 .

For a Tonks gas, all bosonic local observables (such as the energy or the density) are given by those of free fermions. Therefore, since the dynamics of the single-particle orbitals $\psi_i(x, t)$ is that of the non-interacting QKR, we directly infer that they all dynamically localize at long time. The energy (of both fermions and bosons) will thus saturate to a finite value $E_f \simeq E_0 + N \frac{p_{loc}^2}{2}$ for time larger than the localization time, which is interpreted as MBDL [32], see Fig. 1. Since the fermions orbitals reach a steady-state in the MBDL phase, we expect the system to be described by a steady-state density matrix $\hat{\rho}_{ss}$, belonging a priori to the generalized Gibbs

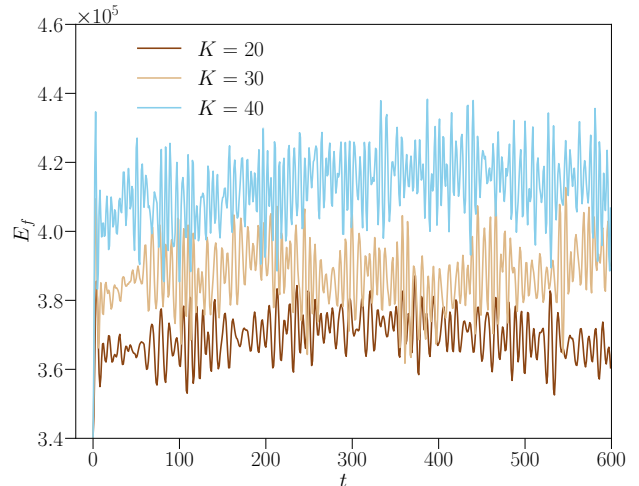


FIG. 1. Time evolution of the total energy of the system $E_f(t)$ for $N = 61$ particles for $K = 20, 30$ and 40 ($k = 6$).

ensemble [33], see discussion in Sec. V. Here we focus on the properties of the system in this MBDL steady state, and thus do not write time dependence of observables.

Non-local observables such as the steady-state one-body density matrix (OBDM)

$$\rho(x, y) = N \int dx_2 \dots dx_N \Psi_B^*(x, x_2, \dots, x_N) \times \Psi_B(y, x_2, \dots, x_N), \quad (3)$$

and its Fourier transform, the momentum distribution

$$n_k = \frac{1}{L} \int dx dy e^{ik(x-y)} \rho(x, y), \quad (4)$$

are significantly different with those of free fermions. Since dynamical localization is a non-local phenomenon, we therefore expect these observables to significantly differ from that of free particles [45]. We therefore focus on those observables in the steady-state (time much larger than the localization time) in the following.

The time-evolution of each single-particle orbital is performed numerically by discretizing space and using Fast Fourier Transform to alternate between real space for the kicks and momentum space for the free propagation. The observables are computed using the method of Refs. [46, 47].

III. MBDL MOMENTUM DISTRIBUTION AND COHERENCE

The groundstate of the Tonks gas is characterized by quasi-long-range order, $n_k \propto 1/\sqrt{k}$ at small momenta and $n_{k=0} \propto \sqrt{N}$, where the sublinear scaling implies the absence of true long-range order [48]. Fig. 2 shows the

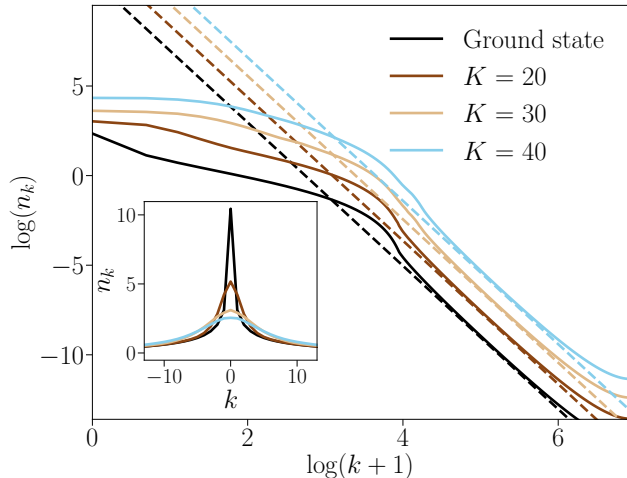


FIG. 2. Steady-state momentum distribution for $N = 51$ particles at $\bar{k} = 6$ for $K = 20, 30$ and 40 in log-log scale (the different n_k have been shifted for better visibility in the main panel). The dashed line shows the asymptotic behavior $n_k \simeq C_{ss}/k^4$ at large momenta, with C_{ss} computed using the effectively thermal density matrix (see text). The inset shows the same quantities in linear scale.

momentum distribution in the ground state and in the localized regime for $N = 51$ bosons, $\bar{k} = 6$ and various values of K , in log-log scale. The divergence at small momenta of the momentum distribution is rounded (see inset), while we observe a power-law decay at large momenta, $n_k \simeq C/k^4$. This behavior is a universal feature of interacting quantum systems, where C is the so-called Tan's contact [35, 36]. We conclude that while the interactions do not destroy dynamical localization, in the sense that the system does not heat up to infinite temperature, they do significantly alter the exponential localization in momentum distribution of the bosons.

The coherence of the Tonks gas in the MBDL regime can also be characterized by the coherence function

$$g_1(r) = \frac{1}{L} \int dR \rho(R - r/2, R + r/2). \quad (5)$$

In its ground state, the gas has algebraic correlations, $g_1(r, t = 0) \propto 1/\sqrt{r}$, corresponding to quasi-long-range order [29]. Fig. 3 shows that in the MBDL regime, the coherence function decays exponentially fast at large distance, implying that the kicks have destroyed the coherence of the quasi-condensate. This is in agreement with the fact that $n_{k=0}$ does not scale with the number of particles (see inset (b) of Fig. 3).

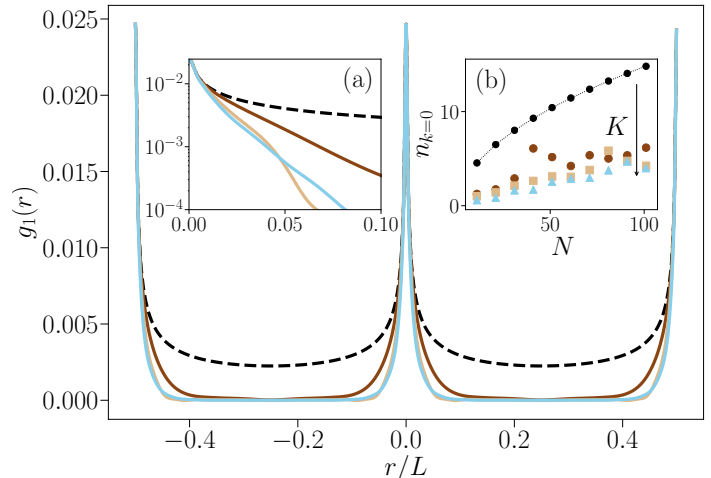


FIG. 3. Steady-state coherence function $g_1(r)$ for $N = 101$ particles at $\bar{k} = 6$ for $K = 20, 30$ and 40 . Inset (a): Same data, in semi-log scale, emphasizing the exponential decay in the MBDL, compared to the $1/\sqrt{r}$ decay of the initial condition (dashed curve); (b): Occupation of the zero-momentum state $n_{k=0}$. It grows as \sqrt{N} in the ground state (dotted line), but saturate to a finite value in the MBDL regime.

IV. EFFECTIVE THERMALIZATION OF MBDL

The absence of quasi-long-range coherence of the localized regime is similar to that of a thermal Tonks gas [29]. We now show that the system is very well described in the MBDL by the a thermal density matrix $\hat{\rho}_{ss} \simeq \hat{\rho}_{th}$, where $\hat{\rho}_{th}$ is the thermal density matrix of the Tonks gas

$$\hat{\rho}_{th} \propto e^{-(\hat{H}_{TGF} - \mu_{eff} \hat{N})/T_{eff}}, \quad (6)$$

with effective temperature T_{eff} and effective chemical potential μ_{eff} that depends on the system's parameters and the number of particles.

Thanks to the Bose-Fermi mapping, if there is indeed effective thermalization, we expect the momentum distribution n_k^F of the underlying free fermions to be described by a Fermi-Dirac distribution, allowing us to extract T_{eff} and μ_{eff} . We therefore begin by analyzing the thermal properties of the free fermions, and then address the thermal-like properties of the Tonks gas in the localized regime.

A. Fermions

An example of the momentum distribution of the fermions in the localized regime is shown in Fig. 4 (symbols). Contrary to the momentum distribution of the bosons, it is rather noisy, as typical for disordered systems. To better fit the momentum distribution of the

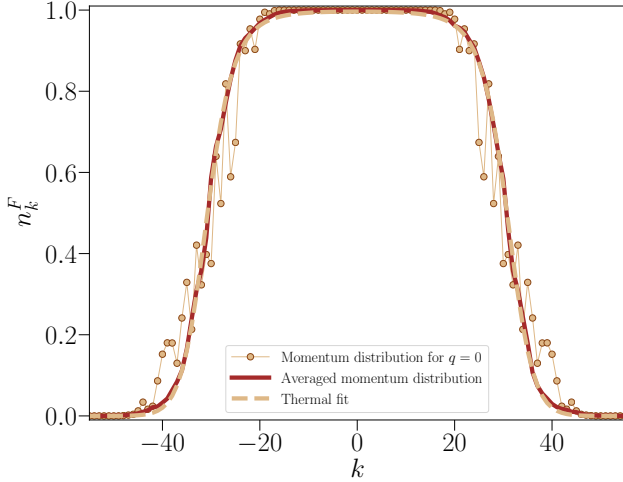


FIG. 4. Comparison between raw and averaged distribution for the many-body momentum distribution. In this case, $N = 61$, $K = 30$, $k = 6$.

fermions, it is convenient to introduce a modified QKR Hamiltonian depending on a parameter q [49]

$$\hat{H}_q = \frac{(\hat{p} + q\hat{k})^2}{2} + K \cos(\hat{x}) \sum_n \delta(t - n). \quad (7)$$

Note that we never average the bosonic observables (we always consider the physical value $q = 0$), such as the OBDM or the momentum distribution. The highly non-linear transformation relating the bosonic observables to that of the fermions averages out the fluctuations. In App. A, we show below that the temperature that can be estimated from $q = 0$ is very well correlated with that extracted from the average fermionic distribution.

In Fig. 4, in addition to the momentum distribution n_k^F at $q = 0$ discussed above, we also show the n_k^F the momentum distribution averaged over 150 random values of q (full line). The smoothing effect of the averaging procedure is very clear. On the same figure, we also show a Fermi-Dirac distribution at an effective temperature T_{eff} and effective chemical potential μ_{eff} such that this thermal distribution explains very well the data (dashed line).

The effective temperature and chemical potential are obtained by imposing that

$$\begin{aligned} \sum_{k \in \mathbb{Z}} f_{FD}(k, T_{eff}, \mu_{eff}) &= N, \\ \sum_{k \in \mathbb{Z}} \frac{k^2 k^2}{2} f_{FD}(k, T_{eff}, \mu_{eff}) &= E_f, \end{aligned} \quad (8)$$

where E_f is the energy obtained from the averaged momentum distribution n_k^F , and f_{FD} is the Fermi-Dirac dis-

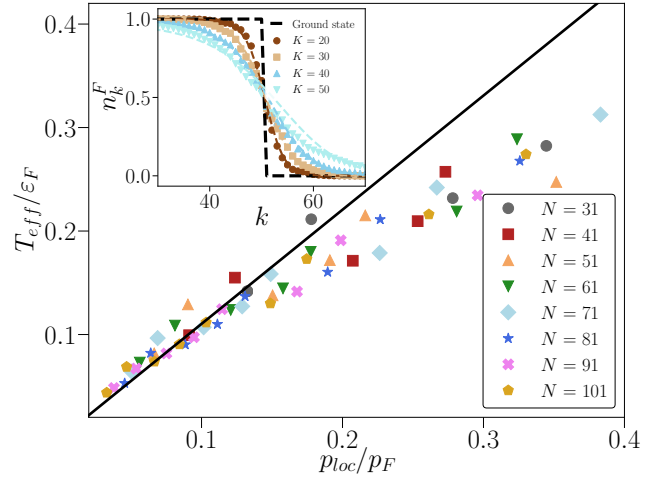


FIG. 5. Effective temperature T_{eff}/ε_F as a function of p_{loc}/p_F for various particle numbers. The collapse of the data shows the linear scaling for small enough p_{loc}/p_F , $T_{eff}/\varepsilon_F \simeq \frac{2\sqrt{3}}{\pi} p_{loc}/p_F$ (black line). Inset: Momentum distribution of the fermions n_k^F in the localized regime (symbols), fitted by a Fermi-Dirac distribution with temperature T_{eff} and chemical potential μ_{eff} , for $N = 101$ and $k = 6$.

tribution

$$f_{FD}(k, T, \mu) = \frac{1}{e^{\frac{k^2 k^2 - \mu}{2T}} + 1}. \quad (9)$$

We observe that the fit is very good, see the inset of Fig. 5, as long as $p_F \gg p_{loc}$ (corresponding to small enough K), see also App. A for a detailed analysis of the parameters regime where the thermal fit works. We focus on this effectively thermal regime here. This corresponds to low effective temperatures compared to the initial Fermi energy $\varepsilon_F = p_F^2/2$, which allows us to find an explicit expression of the effective temperature in terms of the two natural quantities p_{loc} and p_F .

The initial condition of the system corresponds to the ground state, the energy of which is

$$E_0 = \frac{N\varepsilon_F}{3}, \quad (10)$$

for a one-dimensional Fermi gas, with $\varepsilon_F = \frac{p_F^2}{2}$ the Fermi energy, which in our units read $\varepsilon_F = \frac{N^2}{8}$ ($N \gg 1$). On the other hand, in the localized regime, the final energy reads

$$E_f = E_0 + N \frac{p_{loc}^2}{2}. \quad (11)$$

Assuming that the system is thermal, the Sommerfeld expansion of the energy gives

$$E(T_{eff}) \simeq \frac{N\varepsilon_F}{3} + \frac{N\pi^2 T_{eff}^2}{12 \varepsilon_F} + \dots, \quad (12)$$

Equating $E_f = E(T_{eff})$, we obtain

$$\frac{T_{eff}}{\varepsilon_F} = \frac{2\sqrt{3} p_{loc}}{\pi p_F}. \quad (13)$$

Note that the effective temperature is indeed small (compared to the Fermi energy) for small p_{loc}/p_F , validating our initial assumption.

Fig. 5 shows that indeed Eq. (13) works very well for $p_{loc}/p_F \ll 1$. Note that while the effective temperature scales linearly with the particle number, the relative thermal broadening of the Fermi distribution T_{eff}/ε_F vanishes as N^{-1} .

B. Implications for the bosons

Assuming that the steady-state density matrix $\hat{\rho}_{ss}$ is thermal allows us to quantitatively characterize the momentum distribution and the coherence function of the Tonks gas in the localized regime, an a priori formidable task without this insight.

At short distance, the coherence function of a Tonks gas is known to be non-analytic due to the interactions, $g_1(r) \sim \frac{\pi c}{6L} |r|^3$. For a thermal Tonks gas of N bosons at temperature T , the contact reads $\mathcal{C}_{th}(T, N) = \frac{8NE(T, N)}{L^2 k^2}$ [50]. We therefore infer that the contact in the MBDL regime \mathcal{C}_{ss} should be given by $\mathcal{C}_{ss} = \mathcal{C}_{th}(T_{eff}, N)$. Fig. 2 shows that the power-law decay is very well explained by $\mathcal{C}_{th}(T_{eff}, N)/k^4$, showed as dashed lines.

At long distances, the exponential decay of $g_1(r)$ of a Tonks gas at finite temperature, $g_1(r) \propto e^{-2|r|/r_c}$, is also known [29, 51], and in the low-temperature limit we expect $r_c = \frac{kv_F}{T_{eff}}$, where $v_F = \frac{kN}{2}$ is the Fermi velocity in our units. Therefore, due to the effective thermality of the MBDL phase, we expect the correlation length r_c to be independent of the particle number and to be inversely proportional to p_{loc} . Combining the thermal scaling and the expression in Eq. (13), we do expect the scaling $r_c = \frac{\pi}{\sqrt{3}} \frac{k}{p_{loc}}$, which can be rewritten as

$$r_c p_F = \frac{k\pi}{\sqrt{3}} \frac{p_F}{p_{loc}}. \quad (14)$$

Fig. 6 shows good agreement between Eq. (14) and the correlation length extracted from the steady-state (see App. B for details). The inset shows that Eq. (14) describes well the exponential decay of the coherence function.

V. EXPLANATION OF THE EFFECTIVE THERMALIZATION

Let us now argue why the MBDL steady-state appears thermal. This is best understood using the fermionic degrees of freedom, which are non-interacting and evolve

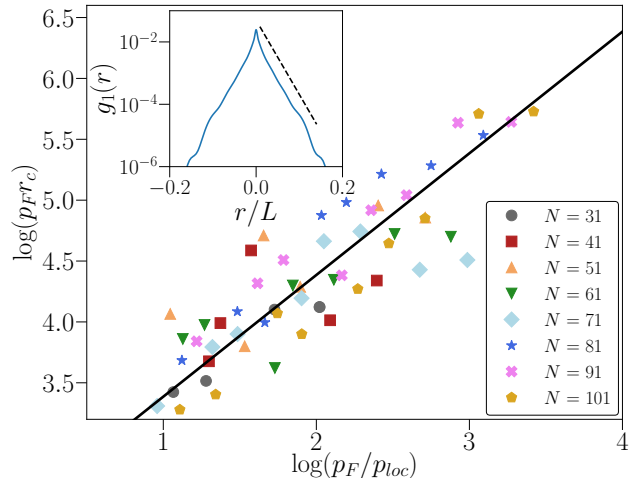


FIG. 6. Correlation length r_c as a function of p_{loc} for various N . The collapse of the data shows that it is independent of the particle number. The line corresponds to the scaling $r_c = \frac{\pi}{\sqrt{3}} \frac{k}{p_{loc}}$. Inset: Coherence function $g_1(r)$ (blue line) and the expected exponential decay with $r_c = \frac{k\pi}{\sqrt{3}p_{loc}}$, for $N = 101$, $K = 40$, $k = 6$.

according to \hat{H}_{QKR} . Introducing the evolution operator over one period \hat{U}_{QKR} and its Floquet eigenstates $\hat{U}_{QKR}|\phi_\alpha\rangle = e^{-i\omega_\alpha}|\phi_\alpha\rangle$, it can be written in second quantization as $\hat{U}_{QKR} = \exp\left(-i\sum_\alpha \omega_\alpha \hat{f}_\alpha^\dagger \hat{f}_\alpha\right)$. Now, the occupation numbers of the Floquet eigenstates $n_\alpha = \langle \hat{f}_\alpha^\dagger \hat{f}_\alpha \rangle$ are obviously constants of motion, and since there is an extensive number of them, the system is integrable. We therefore expect the steady-state to be described by the (periodic) generalized Gibbs ensemble (GGE) [33, 52], $\hat{\rho}_{ss} \simeq \hat{\rho}_{GGE}$, with

$$\hat{\rho}_{GGE} \propto e^{-\sum_\alpha \lambda_\alpha \hat{f}_\alpha^\dagger \hat{f}_\alpha}, \quad (15)$$

where the Lagrange multipliers $\lambda_\alpha = \log((1 - n_\alpha)/n_\alpha)$ are such that $\text{Tr}(\hat{\rho}_{GGE} \hat{f}_\alpha^\dagger \hat{f}_\alpha) = n_\alpha$ [53]. It is a priori surprising that this GGE density matrix, depending on an extensive number of Lagrange multipliers, is well described by a thermal density matrix, depending only on T_{eff} and μ_{eff} . To understand this, we write it in terms of a non-local operator in momentum space

$$\hat{\rho}_{GGE} \propto e^{-\sum_{p,q} M_{p,q} \hat{f}_p^\dagger \hat{f}_q}, \quad (16)$$

with $M_{p,q} = \sum_\alpha \langle p|\phi_\alpha\rangle \lambda_\alpha \langle \phi_\alpha|q\rangle$. Therefore, for generic dynamics and initial states, one should expect a large number of non-local conserved quantities and a clear departure from a thermal state. However, in the present case, we note that the Floquet eigenstates are exponentially localized in momentum space, over a scale of order p_{loc} [9], implying that: (i) only the states with $|p_\alpha| \lesssim p_F + p_{loc}$ are occupied ($n_\alpha \simeq 1$ (resp. 0) for

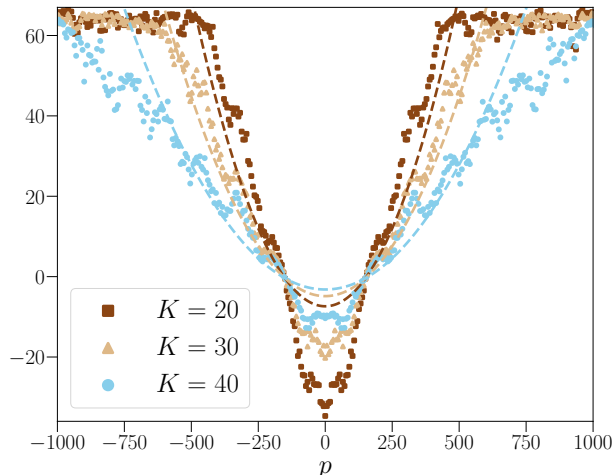


FIG. 7. Comparison of h_p (symbols) with f_p for varying K , $N = 51$ and $\hbar = 6$.

$|p_\alpha| \ll p_F$ (resp. $|p_\alpha| \gg p_F$)), with n_α interpolating between 1 and 0 around $|p_\alpha| \simeq p_F$ on a width of order p_{loc} ; (ii) $M_{p,q} \simeq 0$ if $|p - q| \gg p_{loc}$, meaning that it is almost diagonal, $M_{p,q} \simeq \delta_{p,q} h_p$ for some h_p . In practice, we find that $h_p \simeq f_p \equiv (-\mu_{eff} + p^2/2)/T_{eff}$ to a good approximation as shown in Fig. 7, justifying the effective thermalization $\hat{\rho}_{ss} \simeq \hat{\rho}_{th}$. Note that this effective thermalization depends crucially on point (i), as other initial conditions far from the ground state, or a too large p_{loc} implying that too many eigenstate are populated, do not allow for a description of the steady-state in terms of a thermal density matrix [54].

The fact that $M_{p,q}$ is not exactly diagonal means that the steady state is not perfectly described by a thermal density matrix. In particular, it implies that the natural orbitals of the OBDM are not exactly plane-waves, but have width p_{loc} and that the two-dimensional Fourier transform of the OBDM, $L^{-1} \int dx dy e^{ik(x+y)} \rho(x, y; t)$ decays exponentially as $\exp(-|k|/p_{loc})$ instead of being $N\delta_{k,0}$, see App. C.

VI. CONCLUSION

We have studied the steady-state of a kicked Tonks gas. While dynamical localization is preserved by the interactions, in the sense that the system does not heat up to infinite temperature, we have shown that the momentum distribution of the bosons is not exponentially localized, as in the non-interacting case. Instead, it decays as a power-law given by Tan's contact, as expected for an interacting quantum many-body system. We have

also shown that the steady-state is very well described by a thermal density matrix, with an effective temperature that scales linearly with both the Fermi and localization momenta. This steady-state is therefore both many-body dynamically localized and well described by a small number of constant of motions, corresponding to the particle number and the energy of the localized state, even though the dynamic is integrable, with an extensive number of conserved quantities. This is in contrast with standard MBL, where ergodicity breaking corresponds to emergent integrability and the existence of an extensive set of quasi-local integrals of motion [4]. MBDL should be observable in state-of-the-art cold atoms experiments by measuring the steady-state momentum distribution using for instance the methods of Refs. [55, 56]. As long as the initial temperature is smaller than the effective temperature, effective thermalization should dominate [57]. It can be tested by measuring the momentum distribution of the underlying fermions [58, 59], extracting the corresponding temperature, and comparing with the bosons' observables.

In the few body-limit, it has been shown that finite or infinite interactions give a rather similar dynamical localization of the kicked Lieb-Liniger model [31]. An interesting question is whether this effective thermalization persists beyond the Tonks regime and allows for a quantitative description of the many-body dynamical localization at finite interactions.

Finally, it is well-known that if the kicks strength is modulated, the (non-interacting) QKR displays a delocalization transition similar to the Anderson transition [60, 61], which has been observed experimentally in the atomic QKR [10, 38]. We therefore expect that modulating the kicks in the kicked Lieb-Liniger model will induce a phase transition from the MBDL to a new phase where the system can heat up to infinite temperature. Understanding the properties of such a delocalized phase is under progress.

ACKNOWLEDGMENTS

We thank R. Chicireanu, J.-C. Garreau, D. Delande, N. Cherroret, C. Tian and H. Buljan for insightful discussions. This work was supported by Agence Nationale de la Recherche through Research Grants QRITic I-SITE ULNE/ ANR-16-IDEX-0004 ULNE, the Labex CEMPI Grant No. ANR-11-LABX-0007-01, the Programme Investissements d'Avenir ANR-11-IDEX-0002-02, reference ANR-10-LABX-0037-NEXT and the Ministry of Higher Education and Research, Hauts-de-France Council and European Regional Development Fund (ERDF) through the Contrat de Projets État-Region (CPER Photonics for Society, P4S).

[1] P. W. Anderson, "Absence of diffusion in certain random lattices," *Phys. Rev.* **109**, 1492–1505 (1958).

[2] Ferdinand Evers and Alexander D. Mirlin, "Anderson transitions," *Rev. Mod. Phys.* **80**, 1355–1417 (2008).

- [3] Rahul Nandkishore and David A. Huse, “Many-body localization and thermalization in quantum statistical mechanics,” *Annual Review of Condensed Matter Physics* **6**, 15–38 (2015).
- [4] Dmitry A. Abanin, Ehud Altman, Immanuel Bloch, and Maksym Serbyn, “Colloquium: Many-body localization, thermalization, and entanglement,” *Rev. Mod. Phys.* **91**, 021001 (2019).
- [5] Maksym Serbyn, Z. Papić, and Dmitry A. Abanin, “Local conservation laws and the structure of the many-body localized states,” *Phys. Rev. Lett.* **111**, 127201 (2013).
- [6] David A. Huse, Rahul Nandkishore, and Vadim Oganesyan, “Phenomenology of fully many-body-localized systems,” *Phys. Rev. B* **90**, 174202 (2014).
- [7] Pedro Ponte, Z. Papić, Fran çois Huveneers, and Dmitry A. Abanin, “Many-body localization in periodically driven systems,” *Phys. Rev. Lett.* **114**, 140401 (2015).
- [8] Pedro Ponte, Anushya Chandran, Z. Papić, and Dmitry A. Abanin, “Periodically driven ergodic and many-body localized quantum systems,” *Annals of Physics* **353**, 196–204 (2015).
- [9] Shmuel Fishman, D. R. Grempel, and R. E. Prange, “Chaos, quantum recurrences, and anderson localization,” *Phys. Rev. Lett.* **49**, 509–512 (1982).
- [10] Julien Chabé, Gabriel Lemarié, Benoit Grémaud, Dominique Delande, Pascal Szriftgiser, and Jean Claude Garreau, “Experimental observation of the anderson metal-insulator transition with atomic matter waves,” *Phys. Rev. Lett.* **101**, 255702 (2008).
- [11] Gabriel Lemarié, Hans Lignier, Dominique Delande, Pascal Szriftgiser, and Jean Claude Garreau, “Critical state of the anderson transition: Between a metal and an insulator,” *Phys. Rev. Lett.* **105**, 090601 (2010).
- [12] Matthias Lopez, Jean-Fran çois Clément, Pascal Szriftgiser, Jean Claude Garreau, and Dominique Delande, “Experimental test of universality of the anderson transition,” *Phys. Rev. Lett.* **108**, 095701 (2012).
- [13] Isam Manai, Jean-François Clément, Radu Chircireanu, Clément Hainaut, Jean Claude Garreau, Pascal Szriftgiser, and Dominique Delande, “Experimental observation of two-dimensional anderson localization with the atomic kicked rotor,” *Phys. Rev. Lett.* **115**, 240603 (2015).
- [14] Clément Hainaut, Isam Manai, Jean-François Clément, Jean Claude Garreau, Pascal Szriftgiser, Gabriel Lemarié, Nicolas Cherroret, Dominique Delande, and Radu Chircireanu, “Controlling symmetry and localization with an artificial gauge field in a disordered quantum system,” *Nature Communications* **9**, 1382 (2018).
- [15] Clément Hainaut, Ping Fang, Adam Rançon, Jean-François Clément, Pascal Szriftgiser, Jean-Claude Garreau, Chushun Tian, and Radu Chircireanu, “Experimental observation of a time-driven phase transition in quantum chaos,” *Phys. Rev. Lett.* **121**, 134101 (2018).
- [16] S. Adachi, M. Toda, and K. Ikeda, “Quantum-classical correspondence in many-dimensional quantum chaos,” *Phys. Rev. Lett.* **61**, 659–661 (1988).
- [17] Zhao Wen-Lei and Jie Quan-Lin, “Quantum to classical transition in a system of two coupled kicked rotors,” *Communications in Theoretical Physics* **51**, 465–469 (2009).
- [18] Aydin Cem Keser, Sriram Ganeshan, Gil Refael, and Victor Galitski, “Dynamical many-body localization in an integrable model,” *Phys. Rev. B* **94**, 085120 (2016).
- [19] Efim B. Rozenbaum and Victor Galitski, “Dynamical localization of coupled relativistic kicked rotors,” *Phys. Rev. B* **95**, 064303 (2017).
- [20] Simone Notarnicola, Fernando Iemini, Davide Rossini, Rosario Fazio, Alessandro Silva, and Angelo Russomanno, “From localization to anomalous diffusion in the dynamics of coupled kicked rotors,” *Phys. Rev. E* **97**, 022202 (2018).
- [21] Simone Notarnicola, Alessandro Silva, Rosario Fazio, and Angelo Russomanno, “Slow heating in a quantum coupled kicked rotors system,” *Journal of Statistical Mechanics: Theory and Experiment* **2020**, 024008 (2020).
- [22] Immanuel Bloch, Jean Dalibard, and Wilhelm Zwerger, “Many-body physics with ultracold gases,” *Rev. Mod. Phys.* **80**, 885–964 (2008).
- [23] D. L. Shepelyansky, “Delocalization of quantum chaos by weak nonlinearity,” *Phys. Rev. Lett.* **70**, 1787–1790 (1993).
- [24] A. S. Pikovsky and D. L. Shepelyansky, “Destruction of anderson localization by a weak nonlinearity,” *Phys. Rev. Lett.* **100**, 094101 (2008).
- [25] S. Flach, D. O. Krimer, and Ch. Skokos, “Universal spreading of wave packets in disordered nonlinear systems,” *Phys. Rev. Lett.* **102**, 024101 (2009).
- [26] G. Gligorić, J. D. Bodyfelt, and S. Flach, “Interactions destroy dynamical localization with strong and weak chaos,” *EPL (Europhysics Letters)* **96**, 30004 (2011).
- [27] Nicolas Cherroret, Benoit Vermersch, Jean Claude Garreau, and Dominique Delande, “How nonlinear interactions challenge the three-dimensional anderson transition,” *Phys. Rev. Lett.* **112**, 170603 (2014).
- [28] Samuel Lellouch, Adam Rançon, Stephan De Bièvre, Dominique Delande, and Jean Claude Garreau, “Dynamics of the mean-field-interacting quantum kicked rotor,” *Phys. Rev. A* **101**, 043624 (2020).
- [29] M. A. Cazalilla, R. Citro, T. Giamarchi, E. Orignac, and M. Rigol, “One dimensional bosons: From condensed matter systems to ultracold gases,” *Reviews of Modern Physics* **83**, 1405–1466 (2011).
- [30] Pinquan Qin, Alexei Andreev, Hee Chul Park, and Sergej Flach, “Interacting ultracold atomic kicked rotors: loss of dynamical localization,” *Scientific Reports* **7**, 41139 (2017).
- [31] Radu Chircireanu and Adam Rançon, “Dynamical localization of interacting bosons in the few-body limit,” *Phys. Rev. A* **103**, 043314 (2021).
- [32] Colin Rylands, Efim B. Rozenbaum, Victor Galitski, and Robert Konik, “Many-body dynamical localization in a kicked lieb-liniger gas,” *Phys. Rev. Lett.* **124**, 155302 (2020).
- [33] Achilleas Lazarides, Arnab Das, and Roderich Moessner, “Periodic thermodynamics of isolated quantum systems,” *Phys. Rev. Lett.* **112**, 150401 (2014).
- [34] Lev Vidmar and Marcos Rigol, “Generalized gibbs ensemble in integrable lattice models,” *Journal of Statistical Mechanics: Theory and Experiment* **2016**, 064007 (2016).
- [35] Maxim Olshanii and Vanja Dunjko, “Short-distance correlation properties of the lieb-liniger system and momentum distributions of trapped one-dimensional atomic gases,” *Physical Review Letters* **91**, 090401– (2003).
- [36] Shina Tan, “Large momentum part of a strongly correlated fermi gas,” *Annals of Physics* **323**, 2971 – 2986

- (2008).
- [37] D. L. Shepelyansky, “Localization of quasienergy eigenfunctions in action space,” *Phys. Rev. Lett.* **56**, 677–680 (1986).
- [38] Gabriel Lemarié, Julien Chabé, Pascal Szriftgiser, Jean Claude Garreau, Benoit Grémaud, and Dominique Delande, “Observation of the anderson metal-insulator transition with atomic matter waves: Theory and experiment,” *Phys. Rev. A* **80**, 043626 (2009).
- [39] To be precise, we define p_{loc} of a single-particle state $|\psi\rangle$ as $p_{loc}^2 = \langle \psi | \hat{p}^2 | \psi \rangle - \langle \psi | \hat{p} | \psi \rangle^2$, which is proportional to the momentum scale on which the dynamically localized states decay exponentially.
- [40] M. Girardeau, “Relationship between systems of impenetrable bosons and fermions in one dimension,” *Journal of Mathematical Physics* **1**, 516–523 (1960).
- [41] A. Lenard, “Momentum distribution in the ground state of the one-dimensional system of impenetrable bosons,” *Journal of Mathematical Physics* **5**, 930–943 (1964).
- [42] H. Buljan, R. Pezer, and T. Gasenzer, “Fermi-bose transformation for the time-dependent lieb-liniger gas,” *Phys. Rev. Lett.* **100**, 080406 (2008).
- [43] D. Jukić, R. Pezer, T. Gasenzer, and H. Buljan, “Free expansion of a lieb-liniger gas: Asymptotic form of the wave functions,” *Physical Review A* **78**, 053602– (2008).
- [44] R. Pezer, T. Gasenzer, and H. Buljan, “Single-particle density matrix for a time-dependent strongly interacting one-dimensional bose gas,” *Physical Review A* **80**, 053616– (2009).
- [45] This is to be contrasted with the case of a Tonks gas loaded in a random potential, where localization in real space of the fermions is naturally preserved for the bosons [62, 63].
- [46] Marcos Rigol and Alejandro Muramatsu, “Fermionization in an expanding 1d gas of hard-core bosons,” *Physical Review Letters* **94**, 240403– (2005).
- [47] Marcos Rigol and Alejandro Muramatsu, “Ground-state properties of hard-core bosons confined on one-dimensional optical lattices,” *Physical Review A* **72**, 013604– (2005).
- [48] H. G. Vaidya and C. A. Tracy, “One-particle reduced density matrix of impenetrable bosons in one dimension at zero temperature,” *Phys. Rev. Lett.* **42**, 3–6 (1979).
- [49] The quantity q plays the role of a conserved quasi-momentum in the single-particle QKR without periodic boundary conditions.
- [50] Patrizia Vignolo and Anna Minguzzi, “Universal contact for a tonks-girardeau gas at finite temperature,” *Phys. Rev. Lett.* **110**, 020403 (2013).
- [51] A.R. Its, A.G. Izergin, and V.E. Korepin, “Space correlations in the one-dimensional impenetrable bose gas at finite temperature,” *Physica D: Nonlinear Phenomena* **53**, 187 – 213 (1991).
- [52] Mario Collura, Spyros Sotiriadis, and Pasquale Calabrese, “Equilibration of a tonks-girardeau gas following a trap release,” *Phys. Rev. Lett.* **110**, 245301 (2013).
- [53] The Periodic Gibbs ensemble allows for a time dependence of the steady-state density matrix $\rho_{GGE}(t)$ with $0 \leq t < 1$, with period 1. We only consider here the case $t = 1^-$ (just before the next kick). We have checked that other choices do not change the qualitative picture.
- [54] V. Vuatelet and A. Rançon, to be published.
- [55] A. H. van Amerongen, J. J. P. van Es, P. Wicke, K. V. Kheruntsyan, and N. J. van Druten, “Yang-yang thermodynamics on an atom chip,” *Phys. Rev. Lett.* **100**, 090402 (2008).
- [56] N. Fabbri, D. Clément, L. Fallani, C. Fort, and M. Inguscio, “Momentum-resolved study of an array of one-dimensional strongly phase-fluctuating bose gases,” *Phys. Rev. A* **83**, 031604 (2011).
- [57] Using $T_{eff} \simeq \sqrt{\varepsilon_{loc} \varepsilon_F}$, with ε_{loc} the localization energy per particles, and the estimates $\varepsilon_F \simeq E_R N^2$ and $\varepsilon_{loc} \simeq \alpha E_R$ with E_R the recoil energy and α typically of order a few hundreds depending on the kicks parameters, we estimate that $T_{eff} \simeq 10 N T_R$ ($T_R = E_R/k_B$ the recoil temperature, typically of order $10^{-7} K$ in cold atoms experiments).
- [58] Joshua M. Wilson, Neel Malvania, Yuan Le, Yicheng Zhang, Marcos Rigol, and David S. Weiss, “Observation of dynamical fermionization,” *Science* **367**, 1461–1464 (2020).
- [59] Neel Malvania, Yicheng Zhang, Yuan Le, Jerome Dubail, Marcos Rigol, and David S. Weiss, “Generalized hydrodynamics in strongly interacting 1d bose gases,” *Science* **373**, 1129–1133 (2021).
- [60] D.L. Shepelyansky, “Localization of diffusive excitation in multi-level systems,” *Physica D: Nonlinear Phenomena* **28**, 103 – 114 (1987).
- [61] Giulio Casati, Italo Guarneri, and D. L. Shepelyansky, “Anderson transition in a one-dimensional system with three incommensurate frequencies,” *Phys. Rev. Lett.* **62**, 345–348 (1989).
- [62] J. Radić, V. Bačić, D. Jukić, M. Segev, and H. Buljan, “Anderson localization of a tonks-girardeau gas in potentials with controlled disorder,” *Physical Review A* **81**, 063639– (2010).
- [63] Robert Seiringer and Simone Warzel, “Decay of correlations and absence of superfluidity in the disordered tonks–girardeau gas,” *New Journal of Physics* **18**, 035002 (2016).

Appendix A: Validity of the thermal fit of the steady-state of the fermionic momentum distributions

We focus here on giving details on the effective thermalization and its range of validity with respect to the parameters of the system.

As hinted in the inset of Fig. 5, the thermal fit of the steady-state fermionic momentum distributions works well for $p_{loc}/p_F \ll 1$, while in the opposite limit, it does not work, implying that the system does not effectively thermalize. This can be quantified by introducing the error

$$\varepsilon = \frac{\|n_k^F - f_{FD}(k, T_{eff}, \mu_{eff})\|}{\|n_k^F\|}. \quad (\text{A1})$$

The error as a function of N and K is shown in the top panel of Fig. 8, and as a function of p_F and p_{loc} in the bottom panel. The low value of ε , i.e. a good the thermal fit, corresponds to the blue area in Fig. 8). In the following, we only consider parameters such that $\varepsilon \lesssim 5\%$, where the effective thermalization takes place.

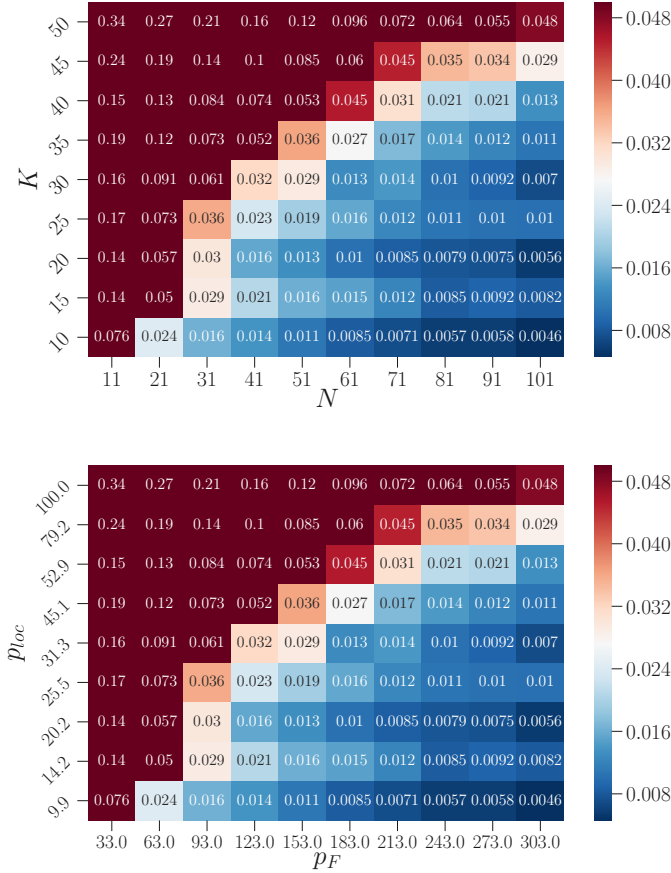


FIG. 8. Top panel: $\varepsilon(N, K)$ at fixed $k = 6$. Dark red color corresponds to $\varepsilon \geq 0.05$. Bottom panel: same as top panel but in function of p_{loc} and p_F .

Fig. 9 shows that the localized energy in the steady-state is well described by the Sommerfeld expansion Eq. (12) in terms of the fitted effective temperature T_{eff} , as long as the temperature is small enough, i.e. when the thermal fit works well (dark blue symbols). Fig. 10 shows that in the same regime, the effective temperature is also well described by our prediction Eq. (13).

Finally, let us address the effects of the averaging over q . Fig. 11 is a scatter plot of $T_{eff}^{(q=0)}$, the effective temperature extracted from the fermionic energy for $q = 0$, and T_{eff} , the effective temperature obtained from the averaged momentum distribution, for various values of N , k and K . We see a very clear correlation between the two. This shows that while averaging is convenient to analyze the fermionic degrees of freedom, the effective temperature and chemical potential obtained will describe very well the non-averaged observables of the bosons.

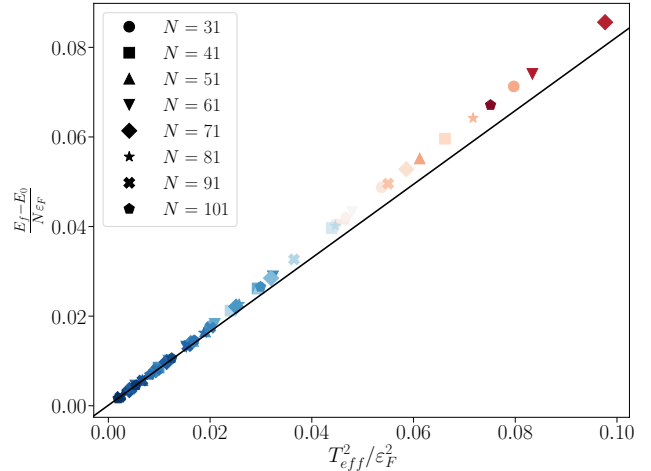


FIG. 9. Final energy E_f as a function of the fitted effective temperature T_{eff} for $k = 6$ and various particle number. In practice, we plot $\frac{E_f - E_0}{N \varepsilon_F}$ as a function of $T_{eff}^2 / \varepsilon_F^2$. The black line corresponds to the Sommerfeld expansion in Eq. (12). The color code corresponds to that of Fig. 8.

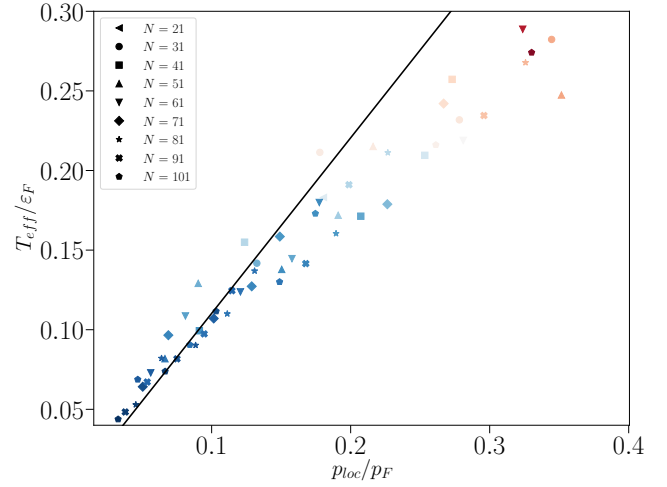


FIG. 10. Effective temperature T_{eff} / ε_F as a function of p_{loc} / p_F for $k = 6$ and various particle number. In practice, we plot $\frac{E_f - E_0}{N \varepsilon_F}$ as a function of $T_{eff}^2 / \varepsilon_F^2$. The black line corresponds to the prediction Eq. (13). The color code corresponds to that of Fig. 8.

Appendix B: Extraction of r_c

We observed that the coherence function of the Tonks gas $g_1(r)$ decays exponentially in the localized regime as it was shown in Fig. 3. Assuming that it decays as $g_1(r) \propto e^{-2|r|/r_c}$, we can estimate the correlation length

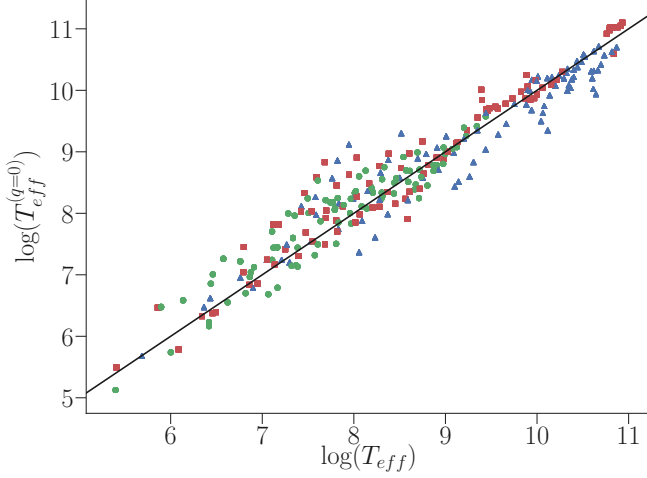


FIG. 11. Comparison of temperature extracted from E_f and from the averaged distribution (respectively $T_{eff}^{(q=0)}$ and T_{eff}). The colored dots are the datas (green: $k = 6$, red : $k = 7$, blue: $k = 8$) and the black line is a guide to the eye. The collapse of the datas around the black line show that $T_{eff}^{(q=0)}$ and T_{eff} are mostly the same.

r_c by

$$r_c = \sqrt{\frac{2 \sum_r r^2 g_1(r) - (\sum_r r g_1(r))^2}{\sum_r g_1(r)}}, \quad (\text{B1})$$

which is well described by Eq. (14) as discussed in the main text, where we have focus on the case $k = 6$. We show in Fig. 12 that for other k , our prediction is in good agreement with the data.

Appendix C: Natural orbitals

The OBDM can be decomposed in natural orbitals $\phi^\eta(x)$, which can be interpreted as the many-body version of the wavefunctions occupied by the bosons, and which are the eigenfunctions of the OBDM,

$$\int dy \rho(x, y) \phi^\eta(y) = \lambda_\eta \phi^\eta(x), \quad (\text{C1})$$

with the λ_η the occupation of η -th natural orbital. Fig. 13 (top) shows the most occupied natural orbital in momentum space for $N = 51$, $K = 20$, $k = 6$ in semi-log scale. We observe that it decays exponentially over a scale p_{loc} , as can be verified by plotting a localized wave-function of the non-interacting QKR (which decays over the same scale).

Fig. 13 (top) shows the two-dimensional Fourier transform of the OBDM,

$$\rho(k, k') = \frac{1}{L} \int dx dy e^{ikx - ik'y} \rho(x, y), \quad (\text{C2})$$

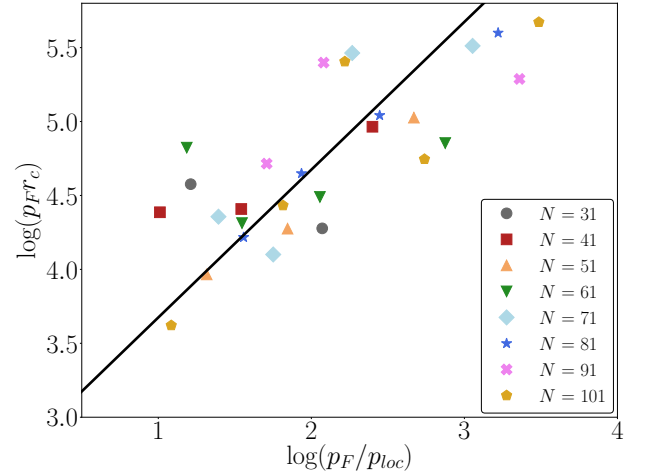
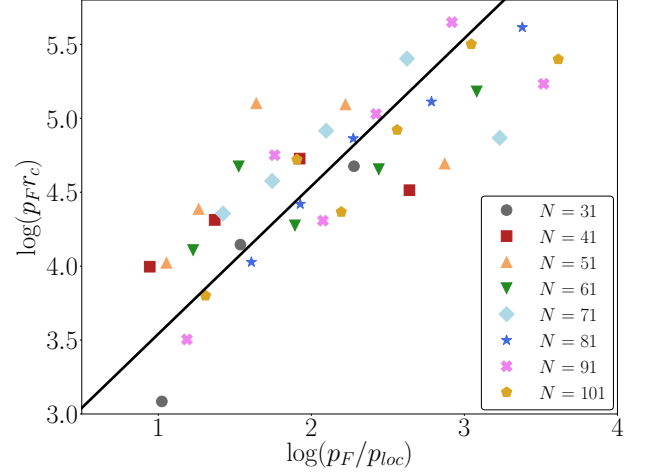


FIG. 12. Correlation length for different k (7, 8 from up to down). The black line correspond on every figure to the relation Eq. (14).

where $\rho(k, k')$ is the momentum distribution. We observe that contrary to a thermal OBDM, it is non-zero for $k \neq k'$ (as expected by invariance by translation for the thermal gas). However, it decays exponentially over the scale p_{loc} , as can be seen in Fig. 13 (bottom).

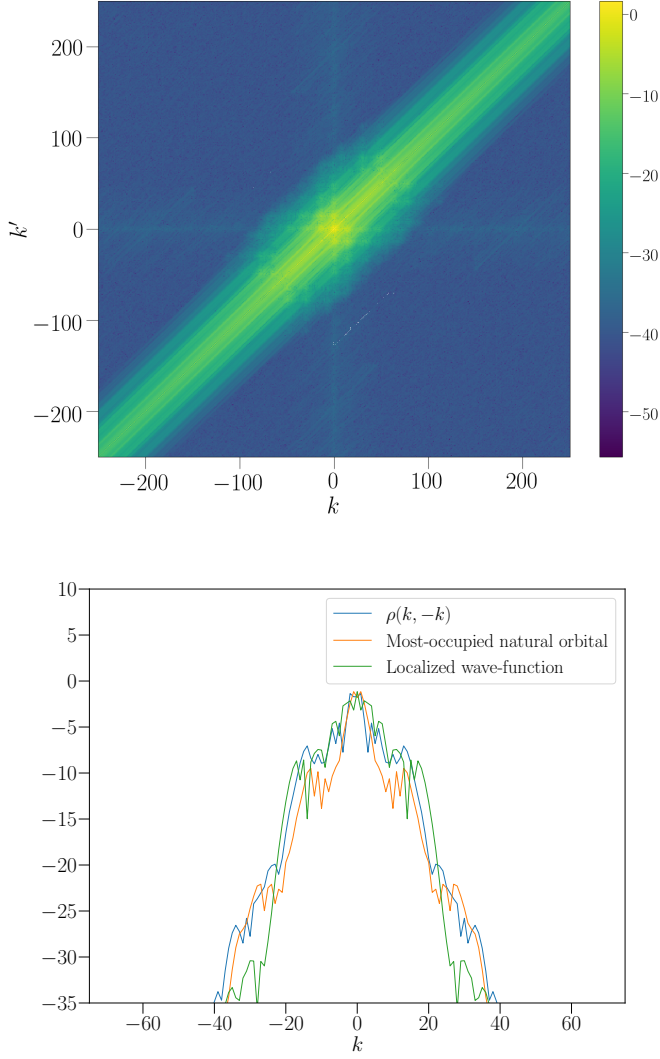


FIG. 13. In both panel $N = 51$, $K = 20$, $\hbar = 6$. Top panel: 2D graphic of the logarithm value of the OBDM in momentum space $\rho(k, k')$. Bottom panel: comparison between the anti-diagonal of the OBDM in momentum space and the most-occupied natural orbitals. We compare them to the $k = 0$ wave-function for the same parameters.